International Journal of Heat and Mass Transfer 174 (2021) 121306

Contents lists available at ScienceDirect

International Journal of Heat and Mass Transfer

journal homepage: www.elsevier.com/locate/hmt

Electroless deposition surface engineering of boron nitride sheets for enhanced thermal conductivity and decreased interfacial thermal resistance of epoxy composites

Yunmin Liang, Bo Zhang, Zhichun Liu*, Wei Liu

School of Energy and Power Engineering, Huazhong University of Science and Technology, Wuhan, 430074, China

ARTICLE INFO

Article history:
Received 15 November 2020
Revised 23 March 2021
Accepted 27 March 2021
Available online 13 April 2021

Keywords:
Polymeric composites
Boron nitride sheets
Electroless deposition surface engineering
Thermal conductivity
Interfacial thermal resistance

ABSTRACT

Filler surface engineering has become an effective method to improve the thermal conduction performance of polymeric composites. However, most of the surface engineering deposits low thermal conductivity materials on the surface of fillers. The increased interfacial thermal resistance between the functional filler will deteriorate the heat transfer capability of thermal conduction network. In order to construct an excellent thermal conduction network, the electroless deposition surface engineering was successfully designed to decorate the surface of BN sheet with high thermal conductivity metallic copper nanoparticles. Through the full characterization of the BN@CuNP and its epoxy-based composites, the effects of electroless deposition surface engineering on thermal conduction enhancement were investigated. The copper nanoparticles deposited on the surface of BN sheets will make the BN@CuNP fillers possess high thermal conductivity and effectively bridge the BN sheets, thereby exhibiting a synergistic effect in reducing the interfacial thermal resistance and enhancing the heat transfer capability of the BN@CuNP thermal conduction network. With the increase of filler content, the effects of electroless deposition surface engineering on thermal conduction enhancement are continuously promoted. The electroless deposition surface engineering shows great advantages in high thermal conductive composites design and fabrication.

1. Introduction

Polymeric composites have shown a vast potential as thermal management materials in electronic package [1,2]. The intrinsic thermal conductivity of polymer matrix is extremely low. Various thermal conductive fillers have been incorporated into the polymer matrix to improve their thermal conductivities [3-6]. The thermal conductive path theory is the most important and versatile theory to reveal the mechanisms of the filled thermally conductive polymeric composites [7,8]. The filler can contact each other to form the thermal conductive filler path, which is the heat transfer path with the minimum thermal resistance in the polymer matrix. The heat flow will effectively transfer along the thermal conductive filler path. When the filler content increases, the adjacent thermal conductive filler paths gradually interact to develop the thermal conduction network, thus improving the thermal conductivity of composites obviously. Large amounts of researches have pointed out that the thermal conduction network constructed by the thermal conductive fillers is the key factor to determine the thermal conduction performance of composites [9-12]. As an important method to improve the formation of thermal conduction network and enhance the heat transfer inside the composites, surface engineering of the thermal conductive fillers has become a research hotspot [13-15]. Diverse surface engineering routes have been used to promote the surface properties of thermal conductive fillers [16-19]. Wang et al. [20] modified the CNT with a dense silica network via the sol-gel method. Compared to the thermal conductivity of blank SR, the thermal conductivity of SR/CNT increased by 17% at one phr (parts per hundreds of rubber) CNT, but the thermal conductivity of SR/SNTs@CNT increased by 130%. The silica-coated CNT has shown great advantages in thermal conductivity enhancement. Inspired by the adhesive proteins in mussels, Liu et al. [21] synthesized PDA coated graphene nanoplatelets and incorporated them into polyvinyl alcohol. The thermal conductivity of PVA/PDA@GnPs composite is significantly higher than that of the PVA/GnPs composite. It is worth noting that most of the surface engineering routes will deposit some low thermal conductivity materials (such as organics and oxide et al.) on the surface

* Corresponding author at: 1037 Luoyu Road, Hongshan District, Wuhan 430074, China.
E-mail address: zcliu@hust.edu.cn (Z. Liu).

https://doi.org/10.1016/j.ijheatmasstransfer.2021.121306
0017-9310/

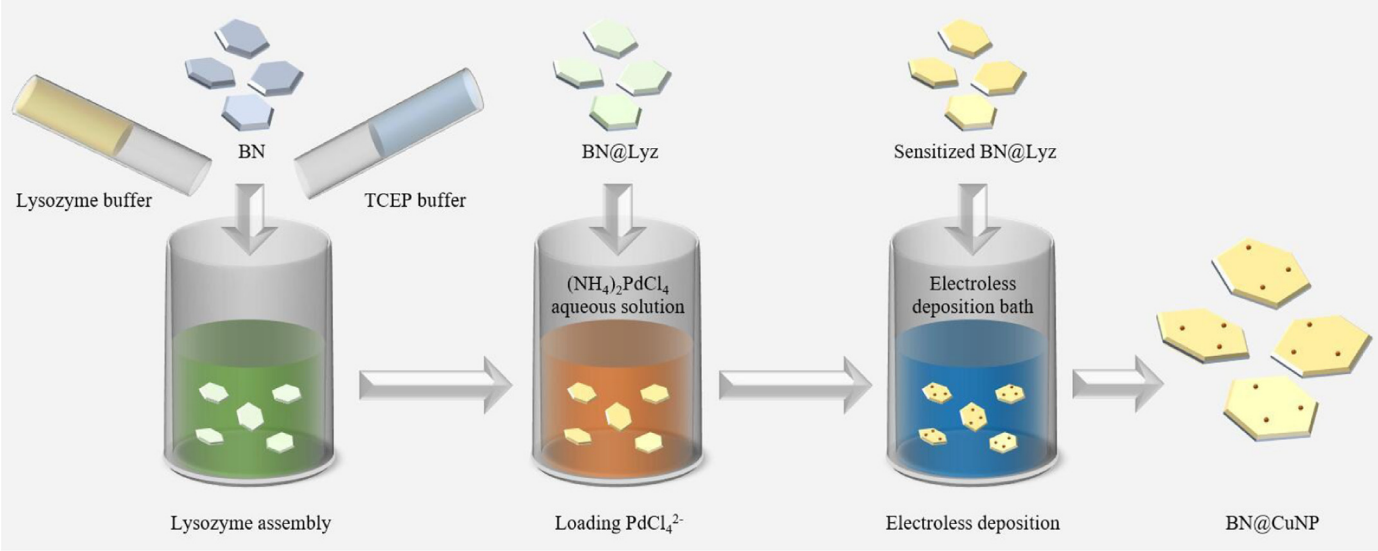

Fig. 1. Schematic diagram of the electroless deposition surface engineering of boron nitride sheets.

of thermal conductive filler. Our previous work [22] has systematically investigated this situation and found that the low thermal conductivity materials used in the surface engineering will increase the interfacial thermal resistance between the thermal conductive fillers and deteriorate the heat transfer capability of thermal conduction network. Compared to the thermal conductivity of composites filled with pristine filler, the effect of composites filled with functional filler on thermal conductivity enhancement will decrease as the filler content increases. When the filler content exceeds the effective filler volume fraction, the thermal conductivity of composites filled with functional fillers is even worse than that of composites filled with pristine fillers. Shen et al. [23] prepared PVA/PDA@BN composites film with aligned structure and the results demonstrated above thermal conduction behavior. Compared to the thermal conductivity of PVA/BN composites film, the thermal conductivity enhancement of PVA/PDA@BN composites film was decreasing with the development of thermal conduction network. When the filler content increased from 10vol.% to 30vol.%, the thermal conductivity enhancement of PVA/PDA@BN decreased from 64% to 21%. In the experiments of Choi [24], compared to the thermal conductivity of TPEE/graphite composites, the thermal conductivity enhancement of TPEE/SiO_2@graphite composites even decreased to -27% at 30wt.%. This negative thermal conduction behavior also can be observed in other material systems [25-27] that deposit low thermal conductivity materials on the surface of thermal conductive fillers to improve the filler surface properties. With the increase of the filler content, the thermal conduction network is gradually formed. However, the enhanced interfacial thermal resistance between the functional thermal conductive fillers significantly deteriorates the effectiveness of filler surface engineering on thermal conductivity enhancement of composites.

In order to reduce the interfacial thermal resistance between the thermal conductive fillers and construct an excellent thermal conduction network inside the composites, some encouraging experiments have tried to modify the filler surface with high thermal conductivity materials. The silver nanoparticle-deposited boron nitride nanosheets [28] and silver nanoparticles anchored reduced graphene oxide [29] prepared by the metal nanoparticle deposition effectively improved the interfacial structure between the fillers and enhanced the thermal conductivities of polymeric composites. The hetero-structured silicon carbide-boron nitride nanosheets [30] synthesized by sol-gel and in-situ growth method exhibited

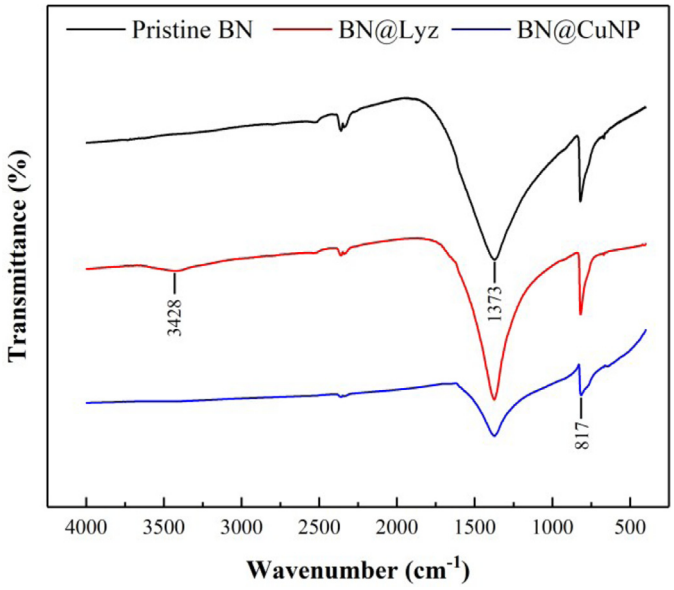

Fig. 2. FT-IR spectra of pristine BN, BN@Lyz, and BN@CuNP.

synergistic improvement effects on the thermal conductivities of the epoxy/SiC-BNNS composites. The copper nanoparticle has received widespread attention due to its high thermal conductivity and low cost and can be deposited on different substrates in a mild way. Herein, a surface engineering based on electroless deposition was designed to decorate BN sheets with the copper nanoparticle. To this end, the pristine BN sheets were first modified via the lysozyme assembly [31,32]. The high isoelectric point (pI=11) of lysozyme will make the surface of BN sheets full of positive charges at neutral pH conditions. Under the electrostatic attraction, the negative $PdCl_4^{2-}$ would be loaded on the surface of BN sheets as a catalyst. Afterwards, in the process of electroless deposition, the copper nanoparticles deposited BN sheets would be yield through the reduction of Cu^{2+} by formaldehyde on the surface of BN sheets [33,34]. Through the full characterization of the BN@CuNP and its epoxy-based composites, the effects of copper nanoparticle deposition surface engineering on thermal conduction enhancement were investigated. With the development of thermal

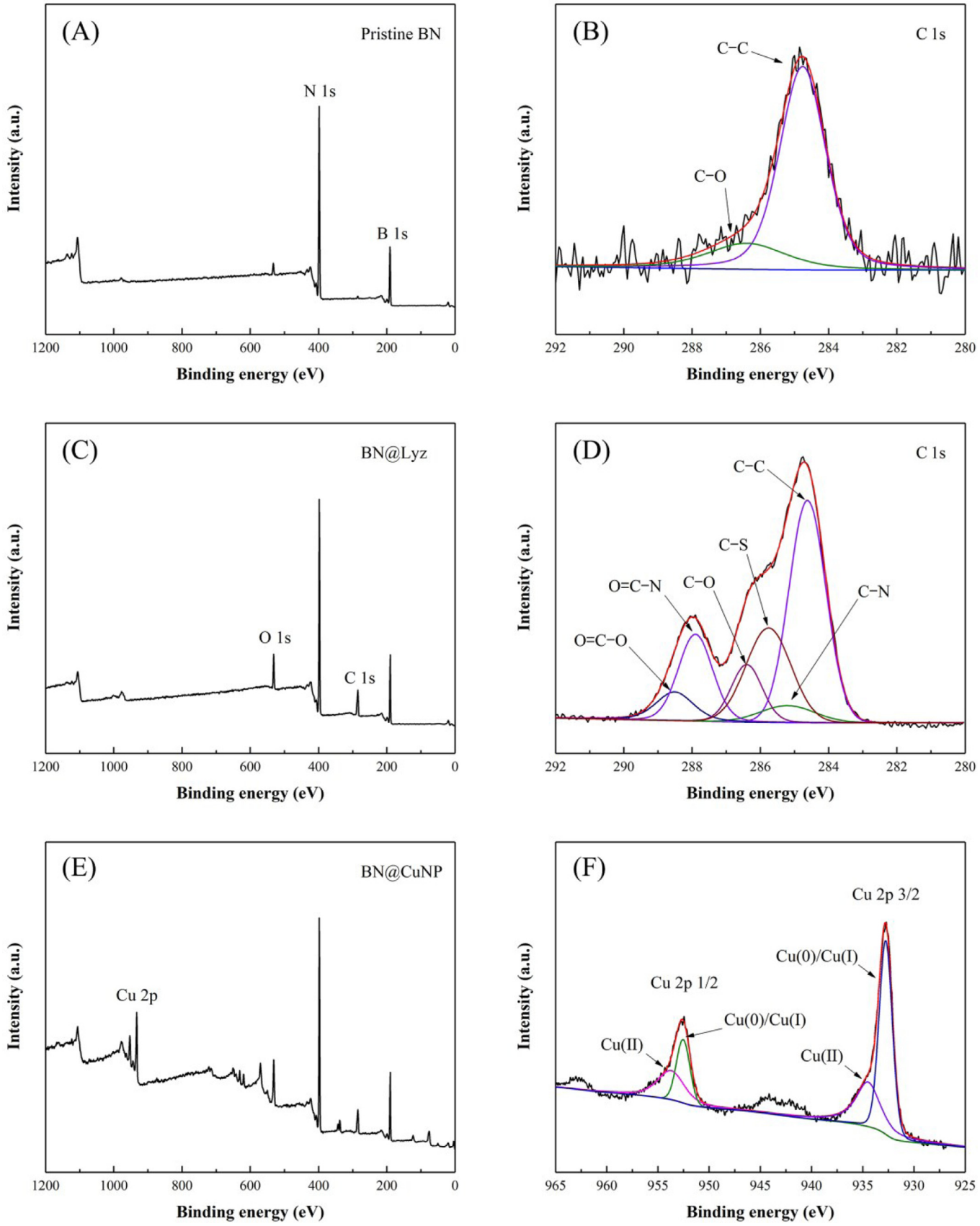

Fig. 3. (A) XPS spectra and (B) high-resolution C 1s spectra of pristine BN; (C) XPS spectra and (D) high-resolution C 1s spectra of BN@Lyz; (E) XPS spectra and (F) high-resolution Cu 2p spectra of BN@CuNP.

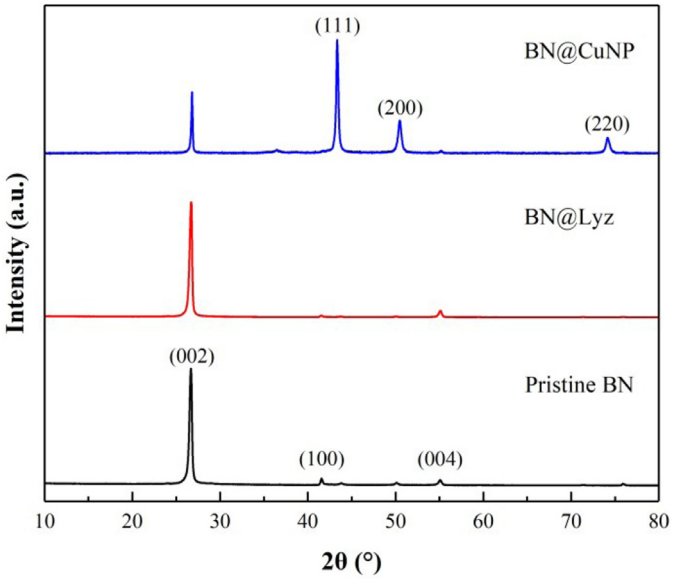

Fig. 4. XRD spectra of pristine BN, BN@Lyz, and BN@CuNP.

conduction network, the reduction of interfacial thermal resistance between the BN@CuNP makes the effect of electroless deposition surface engineering on thermal conduction enhancement increase significantly. The metal electroless deposition surface engineering of fillers provides helpful insight into the rapid and efficient improvement of thermal conductivity of polymeric composites.

2. Experimental work

2.1. Materials

The boron nitride (BN, size of 3~5μm) was purchased from Qinghe Xintie Metal Material Co., Ltd. (Hebei, China). Tris (2-carboxyethyl) phosphine hydrochloride (TCEP) and methyltetrahydrophthalic anhydride (MeTHPA) were purchased from Aladdin. (Shanghai, China). Lysozyme and 4-(2-hydroxyethyl)-1-piperazineethanesulfonic acid (HEPES, pH=7.2~7.4) were purchased from Solarbio. (Beijing, China). Tris (dimethylaminomethyl) phenol (DMP-30) and $(NH_4)_2PdCl_4$ were purchased from the Energy chemical. (Shanghai, China). Sodium hydroxide (NaOH), $CuSO_4{\cdot}5H_2O$, potassium sodium tartrate tetrahydrate, formaldehyde solution (HCHO), ethanol, acetone, and deionized water were purchased from Sinopharm Chemical Reagent Co., Ltd. (Shanghai, China). The epoxy resin diglycidyl ether of bisphenol-A (E-51) with an epoxide equivalent weight of 186 was purchased from Baling Petrochemical Co., Ltd. (Hunan, China). All reagents were used as received without further purification.

2.2. Surface modification of boron nitride via lysozyme assembly (BN@Lyz)

In a typical synthetic process, a certain amount of lysozyme was dissolved in 10mM HEPES buffer to get lysozyme buffer (1mg/mL), and then 1g BN was ultrasonically dispersed into 100mL such freshly prepared lysozyme buffer. Subsequently, a certain amount of TCEP was dissolved in 10mM HEPES buffer to get TCEP buffer (25mM) and the pH of such TCEP buffer was carefully adjusted to 5.0 by 5M NaOH solution. Then 100mL TCEP buffer was added into the above dispersion solution, and the mixture was continuously and mildly stirred for 1h at room temperature. After the reaction, the modified BN, denoted as BN@Lyz, was collected by the vacuum filtration of the above suspension.

2.3. Synthesis of copper nanoparticle-deposited boron nitride sheets (BN@CuNP)

A certain amount of the freshly prepared BN@Lyz was directly immersed into the $(NH_4)_2PdCl_4$ aqueous solution (20mM) for 30 mins. Then the $PdCl_4^{2-}$-loaded BN was collected by vacuum filtration with deionized water several times. The electroless deposition bath consisted of a 1:1 mixture of freshly prepared solution A and B: solution A contained NaOH (10g/L), $CuSO_4{\cdot}5H_2O$ (10g/L), and potassium sodium tartrate (50g/L) in ultrapure water; solution B was HCHO (10ml/L) aqueous solution. Next, the sensitized BN was added into the above electroless deposition bath, and the mixture was mildly stirred at room temperature for 1h. Afterward, the products were collected and washed with deionized water and ethanol sequentially. Finally, the copper nanoparticle-deposited BN sheets were obtained after vacuum drying at 50°C for 24h.

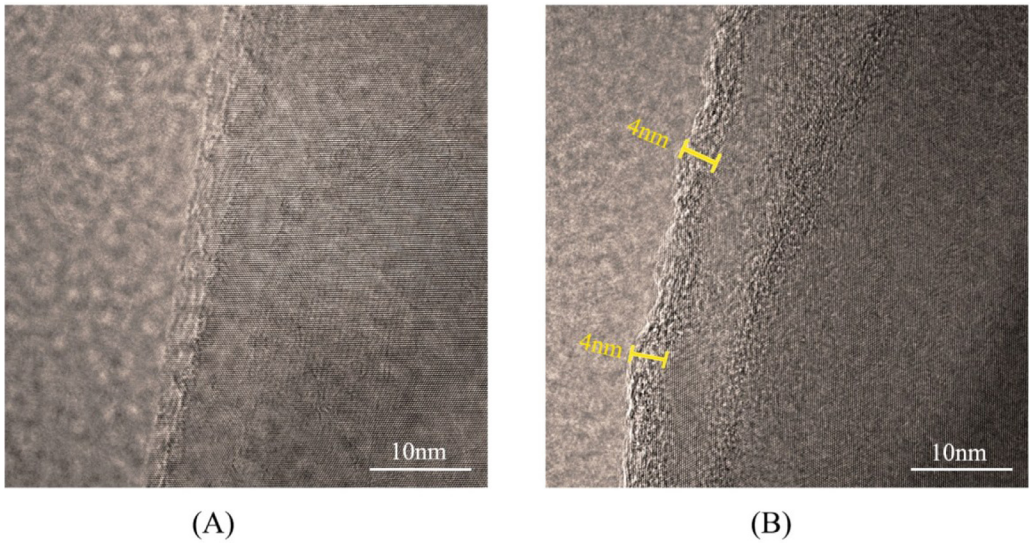

Fig. 5. FETEM images of (A) pristine BN, (B) BN@Lyz.

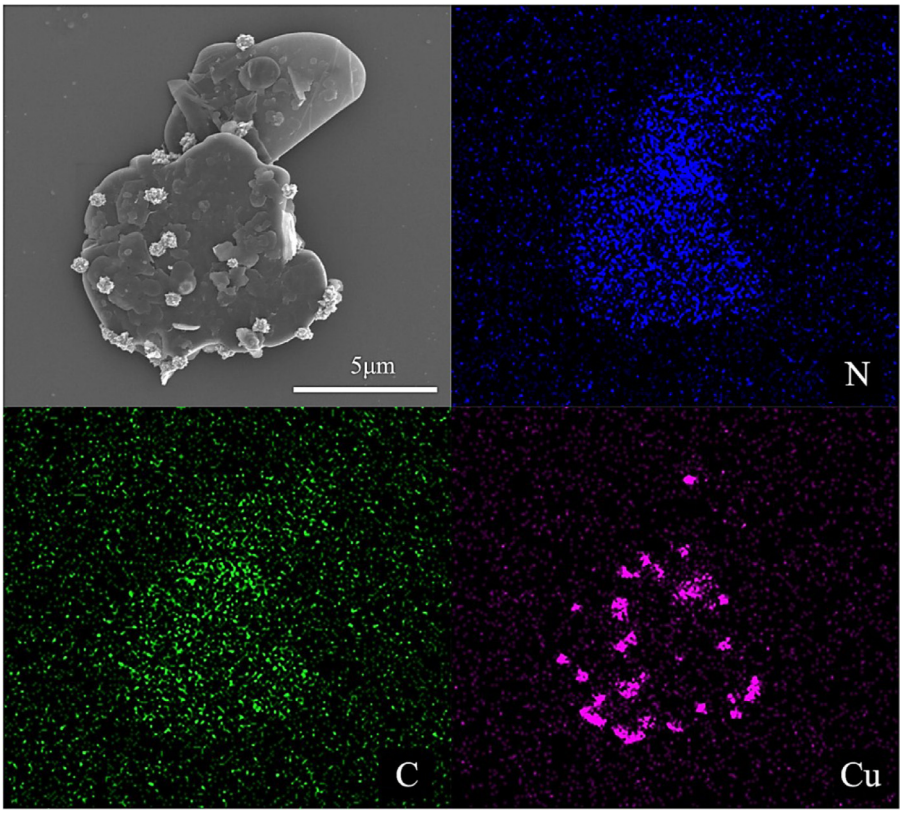

Fig. 6. SEM images of BN@CuNP and element mapping of N element, C element, and Cu element.

2.4. Preparation of epoxy/BN@CuNP composites

Epoxy composites were prepared as follows. 0.7g BN was modified by the electroless deposition surface engineering and then mixed with 3.8g epoxy resin in acetone. After ultrasonic treatment for 2h at room temperature, the obtained blend was vigorously stirred at 60°C until the weight was constant and then combined with 3g MeTHPA and 0.04g DMP-30. Subsequently, the resultant slurry was degassed in a vacuum vessel to remove any trapped air bubbles and residual acetone. Finally, the mixture was cast in steel molds and cured at 80°C for 2 h and 150°C for 4h to form the epoxy/BN@CuNP composite with filler content of 5vol.%. The diameter and thickness of the disc-like sample are 4cm and 2mm, respectively. By controlling the content of BN, a series of composites were prepared. For comparison, the pure epoxy resin and the epoxy/BN composites were prepared following the same procedure described above.

2.5. Characterization

The chemical structures of BN and BN@CuNP were measured by the FTIR spectrophotometer (FT-IR, Bruker Vertex 70, Germany) with the standard KBr pellets method. The morphologies and dispersions of BN and BN@CuNP were observed with scanning electron microscopy (SEM, Sirion200, Netherlands). Energy-dispersive X-ray spectroscopy (EDX, EADX Inc., USA) was used to confirm copper nanoparticles depositing on the surface of BN. Field emission transmission electron microscopy (FETEM, Talos F200X, Netherlands) was used to observe the structure of lysozyme-coated BN. X-ray photoelectron spectroscopy (XPS) was conducted on an ESCALAB 250Xi spectrometer (Thermo Fisher Scientific Inc., USA) to measure the element components on the surface of BN and BN@CuNP. The crystal structure of the BN@CuNP was analyzed using an X-ray diffractometer (XRD, X'Pert3 Powder, Netherlands) with Cu Kα radiation. Thermal conductivity was measured by XIATECH TC3000 thermal conductivity analyzer (Xi'an Xiatech Electronics Co. Ltd., China) by using the transient hot-wire method at room temperature. To reduce the contact thermal resistance between the probe and sample, the surfaces of the cured composites were well polished. Volume resistance of composites was measured by an AR3125 high resistance meter (WanChuang Electronic Co. Ltd., China). The Volume electrical resistivity of the composites was calculated using the formula:

$$\rho_v = \frac{R_v \cdot A}{h} \tag{1}$$

where R_v is the volume resistance (Ω), h is the average thickness of the specimens (cm), A is the effective area of the electrode (cm^2).

3. Results and discussion

3.1. Characterization of BN@CuNP nanoparticles

The schematic diagram of the electroless deposition surface engineering of boron nitride sheets is shown in Fig. 1. The TCEP buffer could effectively break down the disulfide bond to change the lysozyme conformation and induce heterogeneous nucleation and assembly of lysozyme to form a nanofilm at the BN/water interfaces [31,32,35]. Because of the high isoelectric point (pI=11) of lysozyme protein, the lysozyme assembly will make the surface of BN sheets full of positive charges at neutral pH conditions [31]. Then the negative $PdCl_4^{2-}$ could be loaded on the surface of BN sheets by electrostatic self-assembly and acts as an effective catalyst for the electroless deposition of copper nanoparticles [33,34]. Finally, the Cu precursor was reduced to Cu by formaldehyde and deposited on the surface of BN sheets in the electroless deposition bath.

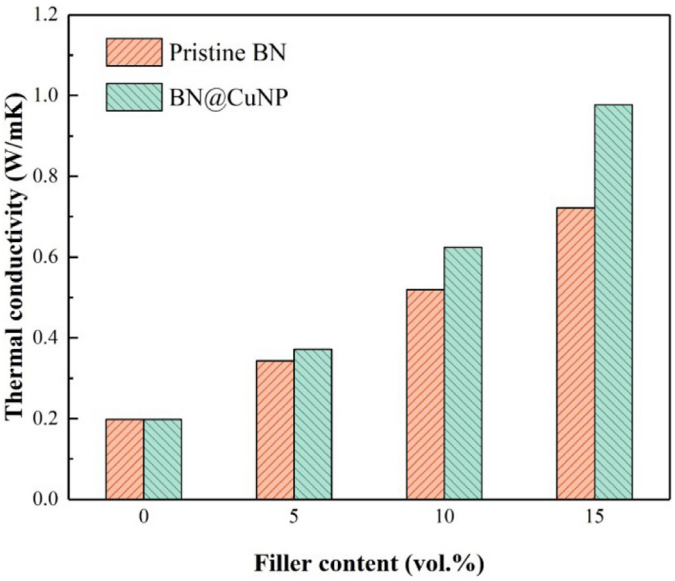

Fig. 7. Thermal conductivities of EP/BN composites and EP/BN@CuNP composites at different filler contents.

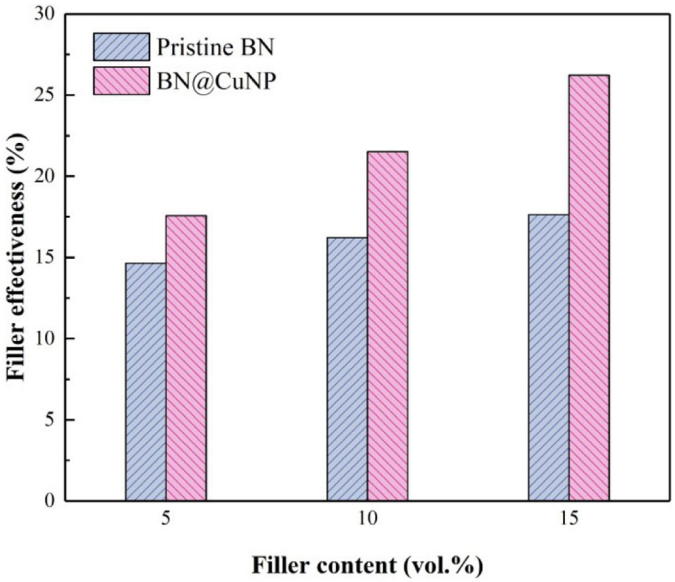

Fig. 8. Filler effectiveness of pristine BN and BN@CuNP at different filler contents.

The chemical structures of BN, BN@Lyz, and BN@CuNP were measured by FT-IR. As shown in Fig. 2, all fillers showed the B-N-B stretching at 1373 cm^{-1} and B-N bending at 817 cm^{-1}. The O-H stretching broad peak appeared at 3428 cm^{-1} in the spectrum of BN@Lyz revealing the existence of lysozyme nanofilm. Compared to the spectrum of BN and BN@Lyz, no new peaks appeared in the spectrum of BN@CuNP but the baseline of the transmission spectrum dropped off heavily at the left, which can be attributed to the infrared light scattering on the rough surface of BN@CuNP. The changes in element components on the surface of pristine BN, BN@Lyz, and BN@CuNP were measured by XPS analysis, and the results are shown in Fig. 3. The peaks at 190, 285, 398, and 532 eV can be assigned to B 1s, C 1s, N 1s, and O 1s, respectively. The weak C 1s signal in the XPS spectra of pristine BN mainly comes from the external contaminant [36]. The high-resolution C 1s spectra of pristine BN can be decomposed into two peaks at 284.8 and 286.4 eV, which can be attributed to C-C and C-O species, respectively. After surface modification via lysozyme assembly, the C 1s signal was obviously increased in the XPS spectra of BN@Lyz. Compared to the high-resolution C 1s spectra of pristine BN, the newly added peaks at 285.2, 285.8, 287.9 and 288.5 eV in the high-resolution C 1s spectra of BN@Lyz can be attributed to the amines (C-N), thiols (C-S), amides (O=C-N) and carboxyl groups (O=C-O) of lysozyme [31,32]. In the XPS spectra of BN@CuNP, the strong Cu 2p signal was recorded and split into Cu 2p 3/2 at 933eV and Cu 2p 1/2 at 953eV, respectively. As shown in Fig. 3(F), copper in the BN@CuNP has two chemical states. The peaks located at 934.5 and 953.8 eV can be attributed to the residual Cu(II) in the electroless deposition. Considering that the metallic copper Cu(0) and copper oxide Cu(I) present very similar signals in XPS, the chemical state from the peaks at 932.8 and 952.6 eV was hard to be identified [37]. Then, the crystal structures of pristine BN, BN@Lyz, and BN@CuNP were analyzed by XRD. As shown in Fig. 4, the diffraction peaks at 26.67°, 41.58°, and 55.06° in the XRD pattern of pristine BN can be indexed to (002), (100), and (004) lattice planes of hexagonal phase. Attributed to the amorphous structure of lysozyme, the BN@Lyz presented the same diffraction peaks as the pristine BN. The intense diffraction peaks appeared at 43.34°, 50.49° and 74.15° in the XRD pattern of BN@CuNP can be indexed to (111), (200), and (220) lattice planes of the face-centered cubic structure of Cu, respectively. The results suggested that the metallic copper has been successfully deposited on the surface of BN.

The surface structure of pristine BN and BN@Lyz were observed by FETEM and the results are depicted in Fig. 5. The surface of pristine BN is smooth and the crystal structure is clear. After surface modification via lysozyme assembly, a thin amorphous lysozyme nanofilm with thickness of 4 nm was coated on the surface of BN. Lysozyme assembly provides multiple functional groups on the surface of pristine BN to support sequential electroless deposition. The morphology of BN@CuNP was observed by SEM and the element mapping was conducted by EDX. As shown in Fig. 6, the metallic copper was evenly deposited as copper nanoparticles on the whole surface of BN. No individual CuNP can be observed in the area, which indicates that all the formed CuNP was anchored on the surface of BN. Moreover, the position of metallic copper nanoparticles deposited on the BN sheets perfectly matched the element mapping of copper and vigorously supported the synthesis of copper nanoparticle deposited BN sheets. Based on the above characterization, the BN@CuNP was successfully synthesized by electroless deposition surface engineering.

3.2. Effects and theoretical analysis of electroless deposition filler surface engineering on thermal conductivity enhancement of composites

The thermal conductivities of epoxy-based composites filled with BN@CuNP are shown in Fig. 7. As the filler content increases, both the thermal conductivities of EP/BN@CuNP composites and EP/BN composites are significantly enhanced. Compared to the thermal conductivity of EP/BN composites, the EP/BN@CuNP composites present a better thermal conduction performance under the same filler content. And the thermal conduction performance gap between two composites obviously increases with the increase of filler content. When the filler content increases from 5vol.% to 15vol.%, the thermal conduction performance gap increases from 0.03W/mK to 0.26W/mK. In order to evaluate the contribution of per part of fillers to the thermal conductivity enhancement, the filler effectiveness (η_f) of pristine BN and BN@CuNP were calculated by the following equation:

$$\eta_f = \frac{k_f - k_r}{k_r V_f} \times 100\% \quad (2)$$

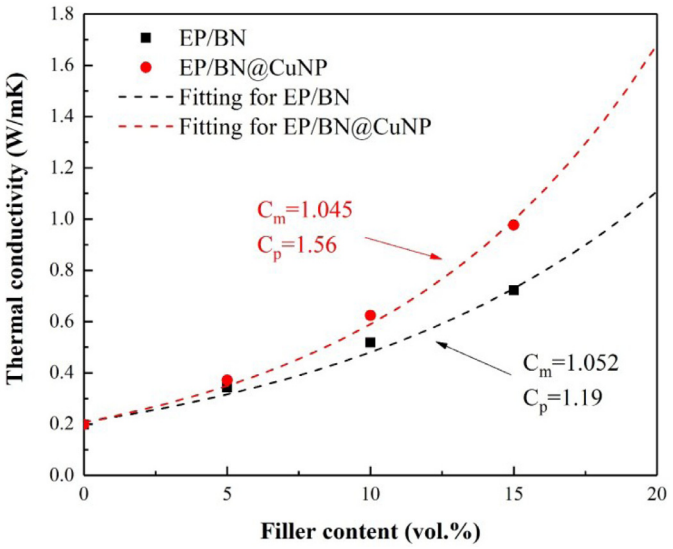

Fig. 9. The experimental value and Y.Agari model fitting curve of the thermal conductivities of EP/BN composites and EP/BN@CuNP composites.

where k_f is the thermal conductivity of composites incorporated with fillers, k_r is the thermal conductivity of resin matrix, V_f is the filler content. The results of filler effectiveness are depicted in Fig. 8. Both the filler effectiveness of pristine BN and BN@CuNP grow up with the increase of filler content that can be attributed to the development of thermal conduction networks. When the filler content is increased, the thermal conductive fillers gradually come into contact with each other to form a thermal conduction network and provide an effective heat flux path. Thus, the thermal conduction inside the composites will get promotion and each part of fillers will make more contributions to thermal conductivity enhancement. However, the filler effectiveness of BN@CuNP grows up faster and the value is higher than the pristine BN under the same filler content. This result suggested that the thermal conduction network constructed by the BN@CuNP has a stronger heat transfer capability.

The effects of electroless deposition surface engineering on thermal conductivity enhancement were analyzed by the Y.Agari model, which considered the formation of thermal conduction paths within the polymer matrix [38,39]. The logarithmic equation of Y.Agari model is given in Eq. (3):

$$logk = fC_p logk_p + (1-f)log(C_m k_m) \tag{3}$$

where C_m represents the effect of the fillers on the polymer crystallinity or crystal size and C_p represents the capability of the fillers to form a thermal conductive chain through the material. As depicted in Fig. 9, the thermal conductivity curves of the composites estimated by the Y.Agari model are fitted very well with the experimental results. The C_m values of EP/BN composites and EP/BN@CuNP composites are 1.052 and 1.045, respectively. The similar C_m values of the two composites suggested that the electroless deposition surface engineering rarely affects the polymer crystallinity or crystal size. However, the C_p values of the two composites have obvious differences. The C_p values of EP/BN composites and EP/BN@CuNP composites are 1.19 and 1.56, respectively. The bigger C_p value of EP/BN@CuNP composites demonstrates that the BN@CuNP has a stronger capability to form a thermal conductive chain through the material. The electroless deposition surface engineering mainly promotes the formation of thermal conduction network to enhance the thermal conductivity of composites.

The copper nanoparticles deposited on the surface of BN sheets make the BN@CuNP fillers possess high thermal conductivity to improve the heat transfer in the composites. Furthermore, the fracture surface morphology and dispersion of BN and BN@CuNP in the epoxy composites gave important insights into the heat transfer in the composites. As shown in Fig. 10, there was no obvious dispersion difference between the pristine BN and BN@CuNP in the

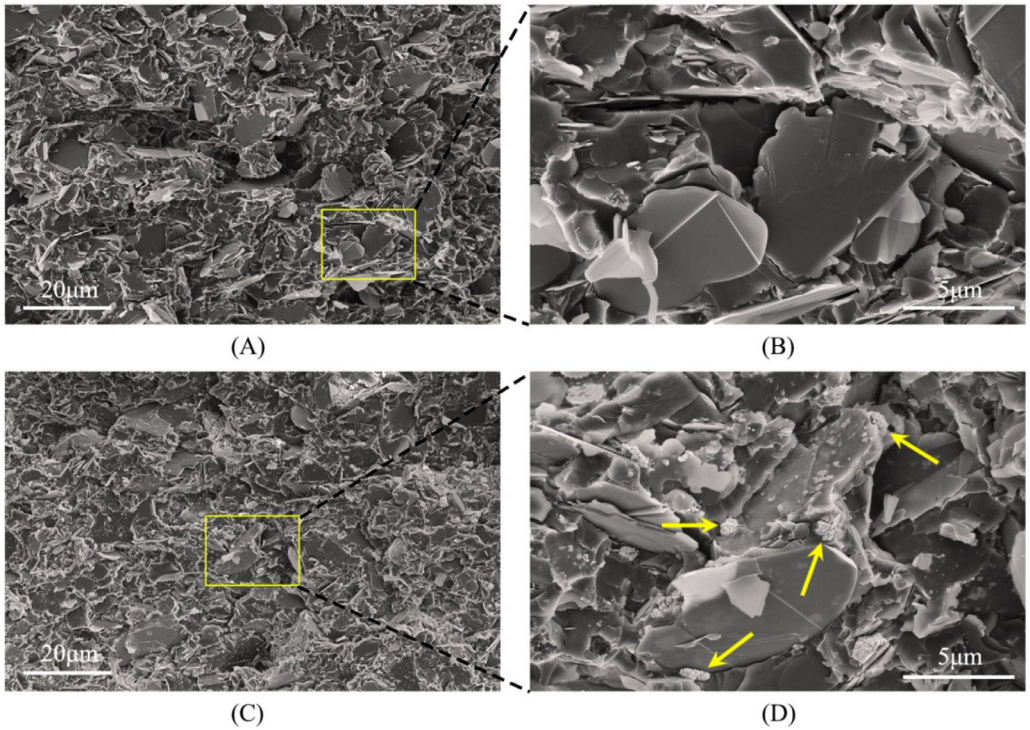

Fig. 10. Fracture surface SEM images of epoxy composites with 10 vol.% pristine BN (A) scale bar is 20μm, (B) scale bar is 5μm; and of epoxy composites with 10 vol.% BN@CuNP (C) scale bar is 20μm, (D) scale bar is 5μm, the arrows show the CuNPs;

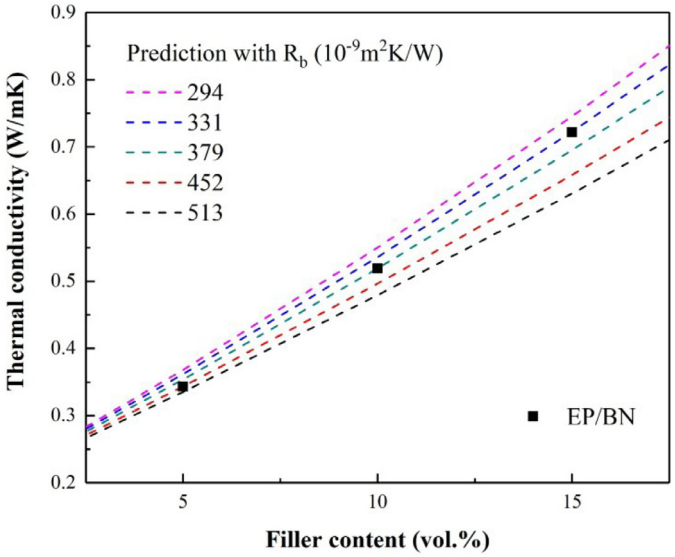

Fig. 11. The measured thermal conductivities (dot) of EP/BN composites and the predicted thermal conductivities (dash line) from EMA with consideration of R_b.

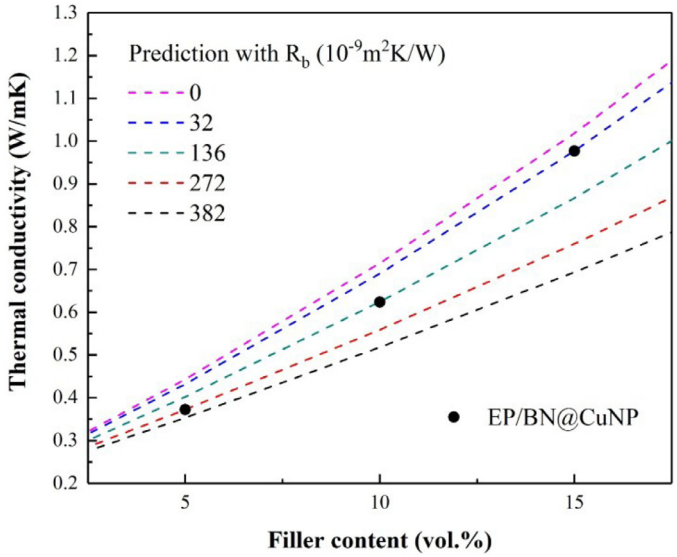

Fig. 12. The measured thermal conductivities (dot) of EP/BN@CuNP composites and the predicted thermal conductivities (dash line) from EMA with consideration of R_b.

epoxy resin. However, the copper nanoparticles deposited on the surface of BN could decrease the gap among the BN sheets and make the BN sheets contact closer with each other. Owing to the high thermal conductivity of metallic copper, the copper nanoparticles bridge the BN sheets to develop the heat flux path, the heat transfer among the BN@CuNP would be more efficient than the pristine BN.

Then, the interfacial thermal resistances inside the composites were calculated by the modified effective medium approximation (EMA), which systematically concerned the effects of intrinsic thermal properties of fillers and matrix, particle geometry, orientation, and interfacial thermal resistance on the thermal conductivity of composites [40]. (The details of the EMA model are presented in the Appendix). By fitting the EMA predictions to the experimental results, the interfacial thermal resistance (R_b) inside the EP/BN composites and EP/BN@CuNP composites at different filler content are extracted and shown in Fig. 11 and Fig. 12, respectively. It's interesting to note that the interfacial thermal resistance inside the two composites reduces significantly with the increase of filler content. The interfacial structure between the fillers and epoxy resin remains consistent at different filler content. As the filler content increases, the interfacial interaction between the fillers becomes stronger to develop the heat transfer path. The reduction of interfacial thermal resistance insider the composite with high filler content can be attributed to the tight filler connection to develop the thermal conduction network. Compared to the R_b inside EP/BN composites, the efficient heat transfer among the BN@CuNP brings the smaller R_b inside EP/BN@CuNP composites under the same filler content. Considering the electroless deposition surface engineering rarely affects the polymer matrix, the smaller R_b inside EP/BN@CuNP composites can be mainly attributed to the reduction of interfacial thermal resistance among the BN@CuNP thermal conduction network. And the effect of electroless deposition surface engineering on interfacial thermal resistance reduction is becoming remarkable with the development of thermal conduction network. The R_b inside EP/BN@CuNP composites is 180 $\times$ $10^{-9}m^2K/W$ smaller than the R_b inside EP/BN composites at 5vol.%, and 299 $\times$ $10^{-9}m^2K/W$ smaller than the R_b inside EP/BN composites at 15vol.%. Thus, as the filler content increases, the BN@CuNP thermal conduction network develops with stronger heat transfer capability, and the thermal conduction performance gap between the two composites is obviously increased. Moreover,

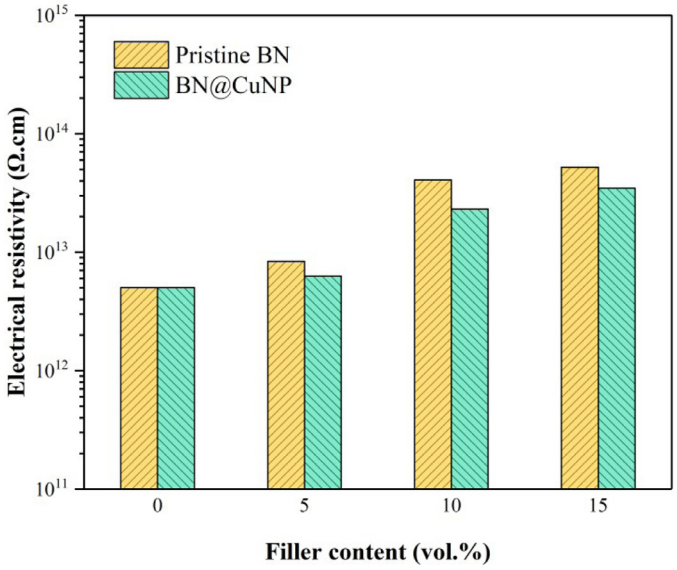

Fig. 13. The electrical resistivity of EP/BN composites and EP/BN@CuNP composites at different filler contents.

the electrical resistivity of two composites was measured and the results are shown in Fig. 13. Compared to the EP/BN composites, the electroless deposition surface engineering will reduce the electrical resistivity of EP/BN@CuNP composites under the same filler content. However, the BN sheets are electrical insulators and provide a tunneling barrier for the electrons. The copper nanoparticles deposited on the surface of BN can not completely form the percolation network, the EP/BN@CuNP composites present good electrical insulation.

The schematic diagrams of thermal conduction inside the EP/BN composites and EP/BN@CuNP composites are shown in Fig. 14. The copper nanoparticles deposited on the surface of BN sheets will make the BN@CuNP fillers possess high thermal conductivity and effectively bridge the BN sheets, thereby exhibiting a synergistic effect in reducing the interfacial thermal resistance and enhancing the heat transfer capability of the BN@CuNP thermal conduction network. With the development of thermal conduction network, the stronger heat transfer capability of BN@CuNP thermal

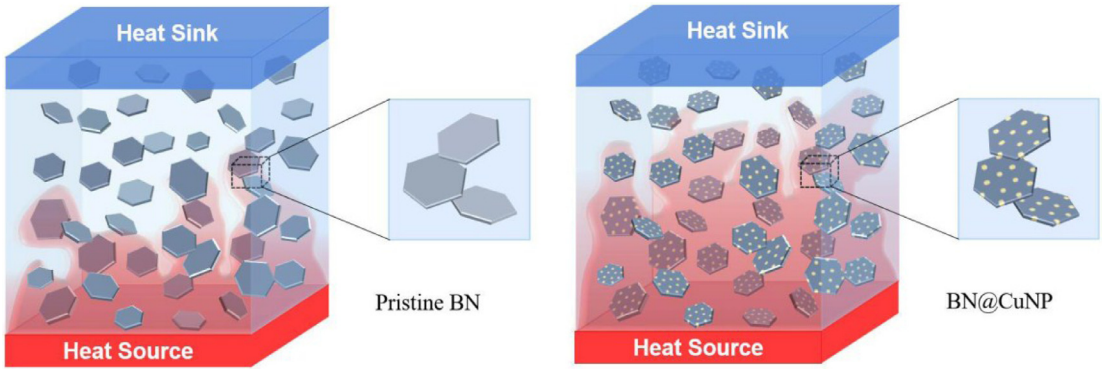

Fig. 14. The schematic diagrams of thermal conduction inside the EP/BN composites and EP/BN@CuNP composites.

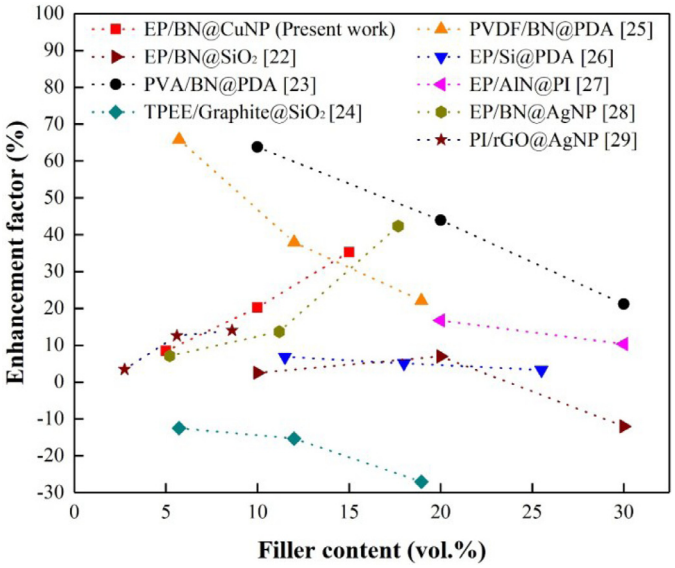

Fig. 15. The enhancement factor of composite systems using different surface engineering.

conduction network will enlarge the effect of electroless deposition surface engineering on thermal conductivity enhancement of composites. Then, the thermal conductive enhancement effect of surface engineering was evaluated by the enhancement factor (η) which can be calculated by the following equation:

$$\eta = \frac{k_s - k_c}{k_c} \times 100\% \quad (4)$$

where k_c is the thermal conductivity of composites incorporated with the pristine filler, k_s is the thermal conductivity of composites incorporated with the modified filler under the same filler content. As shown in Fig. 15, the enhancement factor of electroless deposition surface engineering is compared with different surface engineering and it shows a competitive thermal conductive enhancement effect. The enhanced effect of electroless deposition surface engineering on thermal conduction is continuously promoting with the increase of filler content. The electroless deposition surface engineering shows a great advantage in high thermal conductive composites design and fabrication.

4. Conclusion

In this work, the electroless deposition surface engineering was successfully designed to decorate the surface of BN with copper nanoparticles and the BN@CuNP was subsequently incorporated into the epoxy matrix to yield polymeric composites. The FT-IR, XPS, XRD, SEM, and EDX analyses indicated that Cu nanoparticles were uniformly distributed on the whole surface of BN sheets. The BN@CuNP was shown higher filler effectiveness than that of pristine BN under the same filler content and the thermal conduction performance gap between the two kinds of composites was enlarged as the filler content increased. The electroless deposition surface engineering realized both high thermal conductivity of BN@CuNP fillers and effective connection between the BN sheets, which exhibits a synergistic effect in reducing the interfacial thermal resistance and enhancing the heat transfer capability of the BN@CuNP thermal conduction network. Therefore, the electroless deposition surface engineering significantly promotes the formation of thermal conduction network and the thermal conduction inside the EP/BN@CuNP composites is more efficient. With the development of thermal conduction network, the stronger heat transfer capability of the modified filler thermal conduction network continuously promotes the enhancement factor of electroless deposition surface engineering. Compared with other surface engineering, the electroless deposition surface engineering shows a competitive thermal conductive enhancement effect and provides helpful insight for the high thermal conductive composites design and fabrication.

Declaration of Competing Interest

None declared.

CRediT authorship contribution statement

Yunmin Liang: Conceptualization, Methodology, Validation, Formal analysis, Data curation, Writing - original draft, Writing - review & editing. **Bo Zhang:** Investigation, Validation. **Zhichun Liu:** Resources, Supervision, Project administration, Funding acquisition. **Wei Liu:** Resources, Supervision, Project administration.

Acknowledgements

The research was financially supported by the National Natural Science Foundation of China (No. 51776079, and 51736004).

Appendix

(A) The modified effective medium approximation (EMA) for the prediction of the thermal conductivity of the composites

For the composites filled with particles, the through-plane thermal conductivity (k_{33}) can be expressed as [40]:

$$k_{33} = k_m \frac{1 + f\left[\beta_{11}(1 - L_{11})\left(1 - \left\langle \cos^2\theta \right\rangle\right) + \beta_{33}(1 - L_{33})\left\langle \cos^2\theta \right\rangle\right]}{1 - f\left[\beta_{11}L_{11}\left(1 - \langle \cos^2\theta \rangle\right) + \beta_{33}L_{33}\langle \cos^2\theta \rangle\right]} \tag{A.1}$$

With

$$\beta_{ii} = \frac{k_{ii}^c - k_m}{k_m + L_{ii}\left(k_{ii}^c - k_m\right)} \tag{A.2}$$

$$\left\langle \cos^2\theta \right\rangle = \frac{\int \rho(\theta)\cos^2\theta \sin\theta d\theta}{\int \rho(\theta)\sin\theta d\theta} \tag{A.3}$$

Where 33 and 11 represent through-plane and in-plane direction, respectively. θ is the angle between the composites axis X_3 and the local particle symmetric axis X_3', $\rho(\theta)$ is a distribution function describing particle orientation, and f is the volume fraction of the particles, k_{ii}^c is the equivalent thermal conductivity along the X_{ii}' symmetric axis of the composite unit cell and defined as:

$$k_{ii}^c = k_p / \left(1 + \frac{\gamma L_{ii} k_p}{k_m}\right) \tag{A.4}$$

Where k_m represents the thermal conductivity of the polymer matrix, k_p represents the thermal conductivity of the particles, L_{ii} is geometrical factor dependent on the particle shape. For the platelets,

$$L_{ii} = \frac{p^2}{2\left(p^2 - 1\right)} + \frac{p}{2\left(1 - p^2\right)^{3/2}}\cos^{-1}p \tag{A.5}$$

$$L_{33} = 1 - 2L_{11} \tag{A.6}$$

Where p is the aspect ratio of the particles (for platelets, $p < 1$).

$$\gamma = (1 + 2p)R_b k_m / t \tag{A.7}$$

Where R_b is the interfacial thermal resistance.

(B) The extraction of the interfacial thermal resistance of the composites

For randomly oriented platelets, $< \cos^2\theta >= 1/3$, the thermal conductivity (k) of the composites can be reduced to [40]:

$$k = k_{33} = k_m \frac{3 + f[2\beta_{11}(1 - L_{11}) + \beta_{33}(1 - L_{33})]}{3 - f[2\beta_{11}L_{11} + \beta_{33}L_{33}]} \tag{B.1}$$

Where k_m, k_p and p are input as known parameter: k_m=0.198Wm^{-1}K^{-1}, k_p=300Wm^{-1}K^{-1} [41], the average diameter and thickness of the BN particle are 4μm and 150nm, p=0.0375. Thus, R_b is the only unknown parameter. By calculating the EMA value under different R_b and fitting the predicting curve with the experimental data, the R_b of the composites will be extracted.

References

[1] J. Hansson, T.M. Nilsson, L. Ye, J. Liu, Novel nanostructured thermal interface materials: a review, International Materials Reviews 63 (1) (2017) 22–45.
[2] X. Xu, J. Chen, J. Zhou, B. Li, Thermal Conductivity of Polymers and Their Nanocomposites, Advanced Materials 30 (17) (2018) 1705544.
[3] R.-H. Zhang, X.-T. Shi, L. Tang, Z. Liu, J.-L. Zhang, Y.-Q. Guo, J.-W. Gu, Thermally Conductive and Insulating Epoxy Composites by Synchronously Incorporating Si-sol Functionalized Glass Fibers and Boron Nitride Fillers, Chinese Journal of Polymer Science 38 (7) (2020) 730–739.
[4] X. Yang, J. Zhu, D. Yang, J. Zhang, Y. Guo, X. Zhong, J. Kong, J. Gu, High-efficiency improvement of thermal conductivities for epoxy composites from synthesized liquid crystal epoxy followed by doping BN fillers, Composites Part B: Engineering 185 (2020) 107784.
[5] L. Tang, M. He, X. Na, X. Guan, R. Zhang, J. Zhang, J. Gu, Functionalized glass fibers cloth/spherical BN fillers/epoxy laminated composites with excellent thermal conductivities and electrical insulation properties, Composites Communications 16 (2019) 5–10.
[6] J. Zhang, C. Li, C. Yu, X. Wang, Q. Li, H. Lu, Q. Zhang, J. Zhao, E. Songfeng, M. Hu, Y. Yao, Large improvement of thermal transport and mechanical performance of polyvinyl alcohol composites based on interface enhanced by SiO2 nanoparticle-modified-hexagonal boron nitride, Composites Science and Technology 169 (2019) 167–175.
[7] X. Yang, C. Liang, T. Ma, Y. Guo, J. Kong, J. Gu, M. Chen, J. Zhu, A review on thermally conductive polymeric composites: classification, measurement, model and equations, mechanism and fabrication methods, Advanced Composites and Hybrid Materials 1 (2) (2018) 207–230.
[8] W. Si, J. Sun, X. He, Y. Huang, J. Zhuang, J. Zhang, V. Murugadoss, J. Fan, D. Wu, Z. Guo, Enhancing thermal conductivity via conductive network conversion from high to low thermal dissipation in polydimethylsiloxane composites, Journal of Materials Chemistry C 8 (10) (2020) 3463–3475.
[9] Y. Guo, K. Ruan, X. Shi, X. Yang, J. Gu, Factors affecting thermal conductivities of the polymers and polymer composites: A review, Composites Science and Technology 193 (2020) 108134.
[10] N. Burger, A. Laachachi, M. Ferriol, M. Lutz, V. Toniazzo, D. Ruch, Review of thermal conductivity in composites: Mechanisms, parameters and theory, Progress in Polymer Science 61 (2016) 1–28.
[11] Z. Zhu, C. Li, E. Songfeng, L. Xie, R. Geng, C.-T. Lin, L. Li, Y. Yao, Enhanced thermal conductivity of polyurethane composites via engineering small/large sizes interconnected boron nitride nanosheets, Composites Science and Technology 170 (2019) 93–100.
[12] C. Yu, W. Gong, W. Tian, Q. Zhang, Y. Xu, Z. Lin, M. Hu, X. Fan, Y. Yao, Hot–pressing induced alignment of boron nitride in polyurethane for composite films with thermal conductivity over 50 Wm−1 K−1, Composites Science and Technology 160 (2018) 199–207.
[13] Z. Zheng, M. Cox, B. Li, Surface modification of hexagonal boron nitride nanomaterials: a review, Journal of Materials Science 53 (1) (2017) 66–99.
[14] H. Chen, V.V. Ginzburg, J. Yang, Y. Yang, W. Liu, Y. Huang, L. Du, B. Chen, Thermal conductivity of polymer-based composites: Fundamentals and applications, Progress in Polymer Science 59 (2016) 41–85.
[15] K. Ruan, X. Shi, Y. Guo, J. Gu, Interfacial thermal resistance in thermally conductive polymer composites: A review, Composites Communications 22 (2020) 100518.
[16] W. Stöber, A. Fink, E. Bohn, Controlled growth of monodisperse silica spheres in the micron size range, Journal of Colloid and Interface Science 26 (1) (1968) 62–69.
[17] Y. Jiang, M. Li, C. Chen, Z. Xue, X. Xie, X. Zhou, Y.-W. Mai, Effect of elastic modulus mismatch of epoxy/titanium dioxide coated silver nanowire composites on the performance of thermal conductivity, Composites Science and Technology 165 (2018) 206–213.
[18] H. Lee, S.M. Dellatore, W.M. Miller, P.B. Messersmith, Mussel-Inspired Surface Chemistry for Multifunctional Coatings, Science 318 (5849) (2007) 426.
[19] X. Jiang, P. Ma, F. You, C. Yao, J. Yao, F. Liu, A facile strategy for modifying boron nitride and enhancing its effect on the thermal conductivity of polypropylene/polystyrene blends, RSC Advances 8 (56) (2018) 32132–32137.
[20] Y. Wang, X. Qiu, J. Zheng, Study the mechanism that carbon nanotubes improve thermal stability of polymer composites: An ingenious design idea with coating silica on CNTs and valuable in engineering applications, Composites Science and Technology 167 (2018) 529–538.
[21] Y. Liu, K. Wu, F. Luo, M. Lu, F. Xiao, X. Du, S. Zhang, L. Liang, M. Lu, Significantly enhanced thermal conductivity in polyvinyl alcohol composites enabled by dopamine modified graphene nanoplatelets, Composites Part A: Applied Science and Manufacturing 117 (2019) 134–143.
[22] Y. Liang, B. Liu, B. Zhang, Z. Liu, W. Liu, Effects and mechanism of filler surface coating strategy on thermal conductivity of composites: A case study on epoxy/SiO2-coated BN composites, International Journal of Heat and Mass Transfer 164 (2021) 120533.
[23] H. Shen, J. Guo, H. Wang, N. Zhao, J. Xu, Bioinspired modification of h-BN for high thermal conductive composite films with aligned structure, ACS applied materials & interfaces 7 (10) (2015) 5701–5708.
[24] S. Choi, K. Kim, J. Nam, S.E. Shim, Synthesis of silica-coated graphite by enolization of polyvinylpyrrolidone and its thermal and electrical conductivity in polymer composites, Carbon 60 (2013) 254–265.
[25] D. Zhang, J. Zha, W. Li, C. Li, S. Wang, Y. Wen, Z. Dang, Enhanced thermal conductivity and mechanical property through boron nitride hot string in polyvinylidene fluoride fibers by electrospinning, Composites Science and Technology 156 (2018) 1–7.
[26] Z. Wang, Y. Cheng, M. Yang, J. Huang, D. Cao, S. Chen, Q. Xie, W. Lou, H. Wu, Dielectric properties and thermal conductivity of epoxy composites using core/shell structured Si/SiO2/Polydopamine, Composites Part B: Engineering 140 (2018) 83–90.
[27] Y. Zhou, Y. Yao, C.Y. Chen, K. Moon, H. Wang, C.P. Wong, The use of polyimide–modified aluminum nitride fillers in AlN@PI/epoxy composites with enhanced thermal conductivity for electronic encapsulation, Sci Rep 4 (2014) 4779.
[28] F. Wang, X. Zeng, Y. Yao, R. Sun, J. Xu, C.P. Wong, Silver Nanoparticle-Deposited Boron Nitride Nanosheets as Fillers for Polymeric Composites with High Thermal Conductivity, Scientific Reports 6 (2016) 19394.
[29] Y. Guo, X. Yang, K. Ruan, J. Kong, M. Dong, J. Zhang, J. Gu, Z. Guo, Reduced Graphene Oxide Heterostructured Silver Nanoparticles Significantly Enhanced Thermal Conductivities in Hot-Pressed Electrospun Polyimide Nanocomposites, ACS applied materials & interfaces 11 (28) (2019) 25465–25473.
[30] Y. Han, X. Shi, X. Yang, Y. Guo, J. Zhang, J. Kong, J. Gu, Enhanced thermal conductivities of epoxy nanocomposites via incorporating in-situ fabricated hetero-structured SiC-BNNS fillers, Composites Science and Technology 187 (2020) 107944.

[31] D. Wang, Y. Ha, J. Gu, Q. Li, L. Zhang, P. Yang, 2D Protein Supramolecular Nanofilm with Exceptionally Large Area and Emergent Functions, Advanced Materials 28 (34) (2016) 7414–7423.
[32] R. Liu, J. Zhao, Q. Han, X. Hu, D. Wang, X. Zhang, P. Yang, One-Step Assembly of a Biomimetic Biopolymer Coating for Particle Surface Engineering, Advanced Materials 30 (38) (2018) e1802851.
[33] O. Azzaroni, Z. Zheng, Z. Yang, W.T.S. Huck, Polyelectrolyte Brushes as Efficient Ultrathin Platforms for Site-Selective Copper Electroless Deposition, Langmuir 22 (16) (2006) 6730–6733.
[34] X. Liu, H. Chang, Y. Li, W.T.S. Huck, Z. Zheng, Polyelectrolyte-Bridged Metal/Cotton Hierarchical Structures for Highly Durable Conductive Yarns, ACS applied materials & interfaces 2 (2) (2010) 529–535.
[35] P. Yang, Direct biomolecule binding on nonfouling surfaces via newly discovered supramolecular self-assembly of lysozyme under physiological conditions, Macromol Biosci 12 (8) (2012) 1053–1059.
[36] K. Boumhara, M. Tabyaoui, C. Jama, F. Bentiss, Artemisia Mesatlantica essential oil as green inhibitor for carbon steel corrosion in 1M HCl solution: Electrochemical and XPS investigations, Journal of Industrial and Engineering Chemistry 29 (2015) 146–155.
[37] U. Legrand, R. Boudreault, J.L. Meunier, Decoration of N-functionalized graphene nanoflakes with copper-based nanoparticles for high selectivity CO2 electroreduction towards formate, Electrochimica Acta 318 (2019) 142–150.
[38] Y. Agari, T. Uno, Estimation on thermal conductivities of filled polymers, Journal of Applied Polymer Science 32 (7) (1986) 5705–5712.
[39] Y. Agari, A. Ueda, M. Tanaka, S. Nagai, Thermal conductivity of a polymer filled with particles in the wide range from low to super-high volume content, Journal of Applied Polymer Science 40 (5-6) (1990) 929–941.
[40] C. Nan, R. Birringer, D.R. Clarke, H. Gleiter, Effective thermal conductivity of particulate composites with interfacial thermal resistance, Journal of Applied Physics 81 (10) (1997) 6692–6699.
[41] V. Guerra, C. Wan, T. McNally, Thermal conductivity of 2D nano-structured boron nitride (BN) and its composites with polymers, Progress in Materials Science 100 (2019) 170–186.